School of Physics and Astronomy

Senior Honours Project

Modelling 1-D phonons and disordered lattices with beaded string

Angus Lowe
March 29, 2019

Abstract

1-D phonons are modelled using the normal modes of a steel wire loaded with small masses. The resonant frequencies are measured using a lock-in amplifier, and dispersion relations for both monatomic and diatomic models are shown to agree with theoretical values. Furthermore, localized eigenstates – reminiscent of Anderson localization of electrons – are predicted numerically and verified in the experimental apparatus by introducing disorder to the system. This aspect of the demonstration highlights the tendency of eigenstates in disordered media to decay exponentially on either side of a small region in 1-D.

Declaration

I declare that this project and report is my own work.

Signature: Date:

Supervisor: Professor Malcolm McMahon

Contents

1 Introduction

Phonons are elementary vibrations of a lattice of atoms or molecules at a single frequency, analogous to the normal modes of a classical system[1]. An arbitrary oscillation can be described by a superposition of these phonons, just as waves in a wire are described by its normal modes. Unlike classical modes, however, phonons exhibit particle-like properties for which there are no classical analogues, owing to their quantum nature[2]. For this reason they are considered to be quasiparticles[3], and a treatment of this type yields results which play a role in many phenomena in condensed matter physics. For example, the thermal conductivity and heat capacity of materials depend on the behaviour of phonons[2, 4, 5], as elaborated in Section 3.1. Additionally, interactions between electrons and phonons are thought to be responsible for superconductivity according to BCS theory[6].

In this project, 1-D phonons were modelled using the normal modes of a steel wire loaded with small masses. The system employed a device called a digital lock-in amplifier[7] to drive the vibrations and measure amplitudes, similar to the model described by Lüerßen *et al.*[8] Monatomic and diatomic chains were modelled with the masses representing atoms in a 1-D crystal, and the *dispersion relation* – the relationship between the wavelength and energy of the vibrations – was recorded for various configurations of the experiment. The system was able to demonstrate a variety of phenomena which arise when wavelengths are comparable to distances between neighbouring particles in a medium, and makes apparent that these are not unique to phonons in crystals.

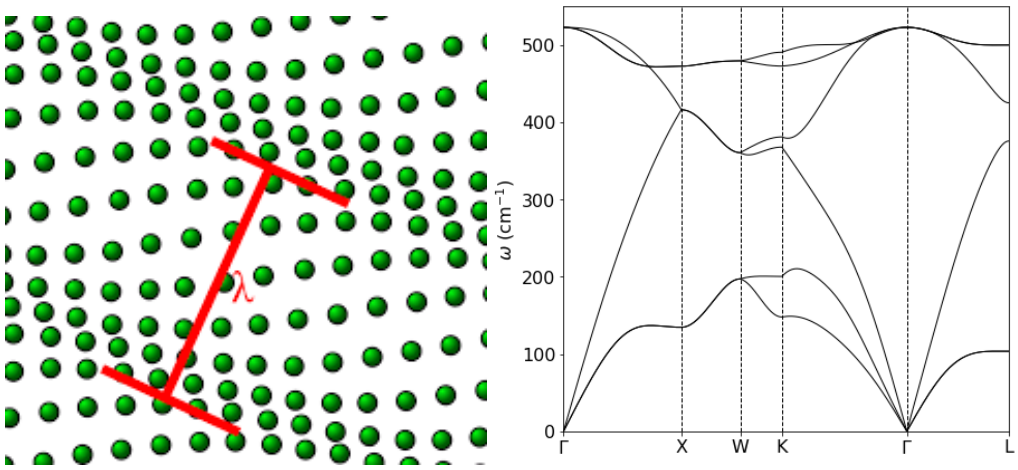

(a) (b)

Figure 1: a) Snapshot of a phonon in a lattice of wavelength λ[9] b) Example of a phonon band structure for crystalline Silicon. Data comes from DFPT calculations performed by the author using the Quantum Espresso software package[10] and ARCHER supercomputing service[11]. The vertical lines indicate points of high-symmetry in the crystal's reciprocal space.

For instance, one feature of any wave travelling in a discrete medium (whether that be atoms or beads on a string of negligible mass) is that linearity of the dispersion relation ceases to hold, such that the group velocity $\partial\omega/\partial k$ differs from the phase velocity ω/k and both become dependent on the frequency[12]. This fact is readily confirmed from the measurements presented in this report and gives insight into behaviour ranging from phonon band structures (see Figure

1) to a single electron in a periodic potential. (Ashcroft and Mermin[12] covers both these topics). Thus, the experiment has pedagogical applications in areas of condensed matter physics (as suggested by Lüerßen *et al.* [8]).

Furthermore, this experiment was able to realize disorder-induced localization of wave packets – reminiscent of Anderson localization in solids[13] – through randomization of the positions of the masses. Anderson localization is the absence of diffusion of waves in a disordered medium and was originally conceived to describe electron localization in a lattice[14], leading to a possible explanation for the metal-insulator phase transition[15]. The consequently localized eigenstates exhibit strong excitations within a confined area and attenuate away from this region exponentially[16, 17]. While Anderson originally found that in 3-D, a specific cut-off value for the amount of disorder exists above which electrons become trapped in their eigenstates, 1-D systems are more amenable to localization effects[13, 17]. In fact, as is elaborated in Section 5, there is no cut-off disorder in 1-D: any level of disorder produces localized eigenstates, given a sufficiently long chain of atoms or beads[18]. With this in mind, the localized eigenstates of the beaded wire system were predicted numerically and then measured experimentally with the lock-in amplifier.

Demonstrating localization phenomena using oscillations of beads on a wire is not an original idea and has been pursued in its own right[19, 20] and for the purposes of modelling inelastic scattering effects due to Anderson Localization of electrons[21]. Localization is ubiquitous in disordered media and has been seen in phenomena as far-reaching as the expansion of cold atoms, scattering of visible light, and acoustic excitations[22] (see Figure 2). The trapping of energy associated with localization phenomena can even lead to unintended engineering consequences, as in the case of bladed disks which are used in aerospace design. (This is mentioned by Ottarsson and Pierre[19] and explored further by Valero and Bendikson[23] and by Wei and Pierre[24].) Most recently, a collaboration was able to demonstrate experimentally the localization of phonons involved in heat conduction[25].

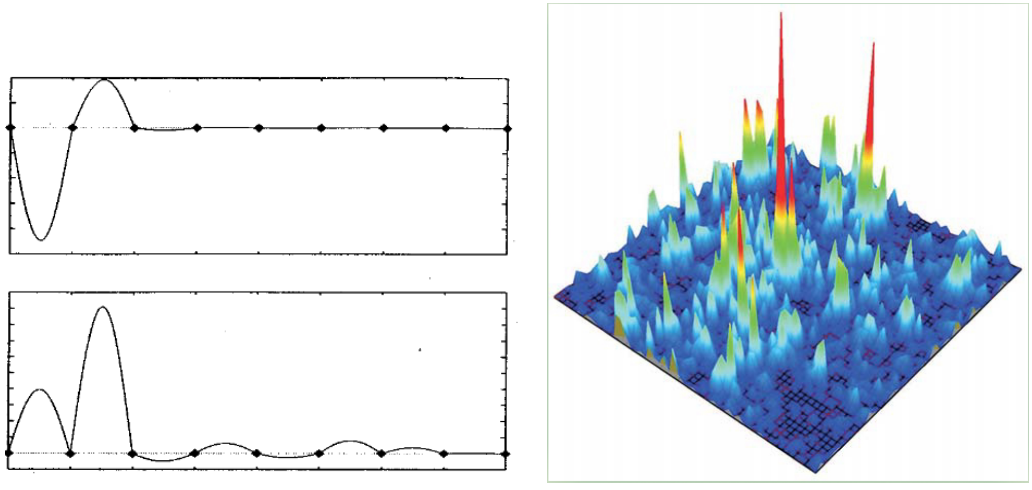

(a) (b)

Figure 2: a) Localized eigenstate of a vibrating wire with seven beads acting as scatterers[19]. b) Energy density of 2.4 MHz elastic waves localized in 3D network of beads[22].

2 Bare string

2.1 Vibrations in bare string

This section provides a review of the terminology and theory for 1-D standing waves on a string. (The terms *string* and *wire* will be used interchangeably in this report.) The treatment is standard in many textbooks, such as in Boas[26]. The 1-D wave equation for an ideal string is

$$\frac{\partial^2 y}{\partial x^2} = \frac{1}{v^2}\frac{\partial^2 y}{\partial t^2} \tag{1}$$

where y represents the transverse displacement, $v = \sqrt{T/\mu}$ for a stretched string, μ is the mass per unit length, and T is the tension in the string. This equation admits solutions of the form

$$y(x,t) = A\sin(kx \pm \omega t)$$

with the convention that $\omega = 2\pi f$, $k = 2\pi/\lambda$, f is the frequency of vibration, λ is the wavelength, and the linear relation $v = \omega k$ holds. Applying the boundary conditions $y(0,t) = y(L,t) = 0$ results in standing waves, also known as the normal modes of vibration for a finite string of length L, and the following constraint on the values of the wavenumber k:

$$k_n = \frac{n\pi}{L},\ n = 1, 2, ... \tag{2}$$

These vibrational modes of the stretched string will respond to being driven at their natural frequencies $\omega_n = vk_n$, and this resonance behaviour can be detected using a lock-in amplifier as described in Sections 2.2 and 2.3.

2.2 Lock-in amplifier

In this project, the Stanford Research SR830 digital signal processing (DSP) lock-in amplifier[7, 27] was used to measure the amplitude and phase of vibrations in a steel wire. Such a device is able to measure amplitudes of a signal matching a specific reference frequency *and* phase while ignoring external noise (signals with a different frequency or phase). A pair of magnetic transducers are used to both drive and detect vibrations in the steel wire through a varying voltage supplied by the amplifier's internal oscillator. Therefore, the reference frequency and phase for the lock-in amplifier are synchronised to the excitation from its internal oscillator to detect signals originating from the driver. By scanning through the driving frequency, it is possible to detect the normal modes of vibration (resonance frequencies) through observation of a significant peak in the output amplitude. Figure 3 displays the functional circuit diagram of the device.

Though not directly relevant to the results, the underlying mechanism of the lock-in amplifier is briefly outlined because the device was an integral component of the project. The goal of the amplifier is to extract the strength of a pure sine-wave signal at the reference frequency. Mathematically, the device seeks to determine the component of the Fourier series whose frequency matches the reference. Consider an arbitrary signal which is periodic with frequency ω.

$$f(t) = \frac{b_0}{2} + \sum_{n=1}^{\infty} b_n \sin(n\omega t + \phi_n)$$

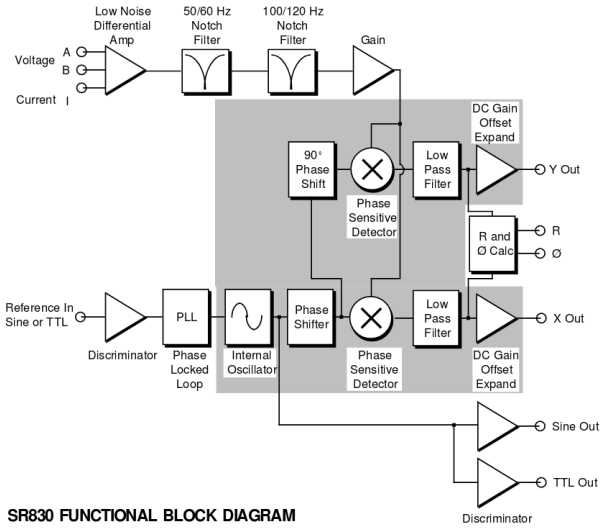

Figure 3: Functional circuit for SR830 lock-in amplifier[27].

The device, locked to frequency ω and phase ϕ_1, multiplies the signal by the reference signal $\sin(\omega t + \phi_1)$ and takes the average of this product[27]

$$f(t) \to \langle f(t) \sin(\omega t + \phi_1) \rangle \tag{3}$$

Now, using orthogonality of the sine function

$$\langle \sin x \rangle = 0, \ \langle \sin x \sin y \rangle = \frac{1}{2} \delta_{xy}$$

Therefore, the only term that survives the multiplication is $n = 1$ so that the measured signal is given by $b_1 \sin(\omega t + \phi_1)$ and not the original signal $f(t)$ which would be measured, for example, on an oscilloscope[27]. The final step is a low-pass filter after the multiplication to remove signals at other frequencies ω'. (See Figure 3 and documentation[27].) The SR830 displays the measured signal in Volts RMS as elaborated in the documentation for the device.

2.3 Experimental setup

The steel wire was strung between 2 clamps on the mount as shown in Figure 4. The wire was extended over 2 knife-edges, which made the effective length of the wire the distance between these 2 edges. Tension was applied to the wire through a lever connected to one of the clamps, which could be used to extend the wire. A weight was attached to this lever, resulting in a constant tension. The lever was designed in such a way that the tension could be deduced by multiplying the rung of the lever by the weight. A 1 kg weight was fixed to the 5th rung of the lever, resulting in a constant tension of $T = 49 \pm 0.5$ kg. The length of the steel wire was $L = (2.363 \pm 0.001)$ m as measured from one knife-edge to the other, beginning at 0.30 m along the mount and ending at 2.663 m. (The distance along the mount was indicated on its side, so that measurements of position are in terms of the distance along the mount.)

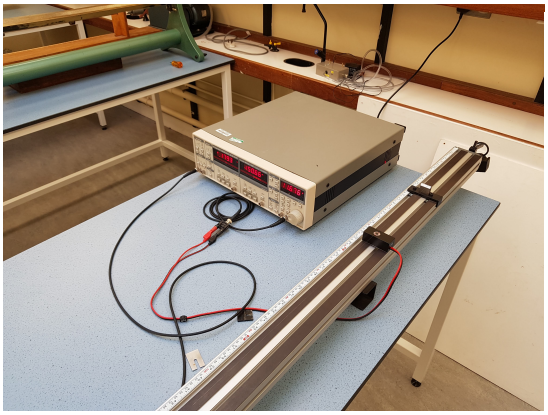

(a)

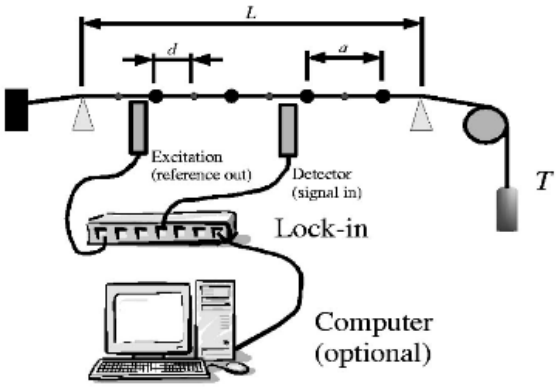

(b)

Figure 4: a) The digital lock-in amplifier and bare steel wire setup. The lock-in amplifier provides both the driving frequency and signal detection with little noise. b) Schematic of experiment setup from the Lüerßen *et al* article[8]. For the first experiment using a bare wire, no beads were attached.

The eigenfrequencies of the bare steel wire were measured with the lock-in amplifier by tuning the driving frequency and reading off the output amplitude data from the detector[1]. The amplitude shows a Lorentzian peak and is orders of magnitude higher at a frequency corresponding to a normal mode of vibration. To determine the resonance frequency, the driving frequency is increased so long as the amplitude increases. The value of the driving frequency for which the amplitude begins to decrease is recorded as a resonance frequency. The time constant was fixed at 3 s throughout, and the sensitivity of the detector was 500 μV.

As in Figure 4, the driver (closer to the knife-edge) is placed a distance of 22.3 cm from one of the knife-edges. The position of the detector on the other hand (device with red and black wires feeding into it) is adjusted for the purposes of error estimation, as described below. The magnetic transducers used to drive the wire are supplied with a sinusoidal voltage and attract the wire for both negative and positive voltages. Therefore, the wire is actually excited at 2 times the driving frequency. Measurements in figures are updated accordingly such that the data is displayed as 2ω instead of ω, the observed angular frequency. Additionally, the detector was set to the 2nd harmonic of the driving frequency to detect the vibrations originating from the internal oscillator.

Error estimation in the bare string was performed by adjusting the position of the detector and repeating the experiment to look for the resonance frequency. Since this frequency does not, in theory, depend on the position of the detector along the mount, the discrepancy in measurement values provides an estimate of the error. Data points for which an error is calculated are plotted using the mean value of the measurements. The uncertainty in determining the amplitude (or phase) against driving frequency for a fixed position was obtained by taking the most frequently displayed value for the output voltage (or phase) and recording the largest deviation from this value.

[1]The amplitude and phase against frequency are displayed in Figure 9 in Section 3, which shows the characteristic resonance behaviour of a system being driven at one of its natural frequencies.

2.4 Results

The aim of the bare string analysis is to show a linear relationship between the vibrational frequency and the wave number as in the expression below

$$\begin{aligned} \omega &= \sqrt{\frac{T}{\mu}}k \\ &= \frac{\pi}{L}\sqrt{\frac{T}{\mu}}n, \ n = 1, 2, ... \end{aligned} \tag{4}$$

where μ is the linear mass density of the wire, L is the length of the wire, T is the tension, and n is the mode number i.e. the number which parameterizes the discrete values of the wavevector, k. A plot of the dispersion relation for this stretched wire is shown in Figure 5, and it can

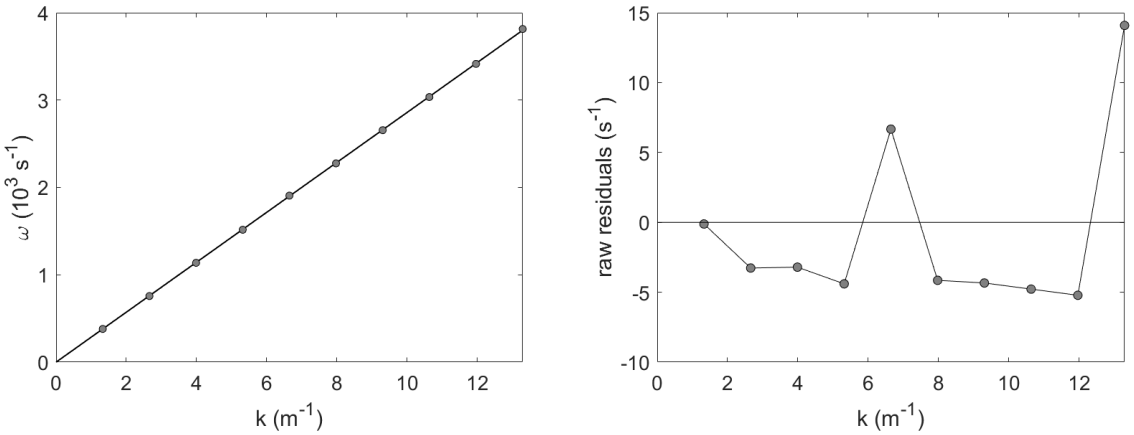

(a) (b)

Figure 5: (a) Dispersion relation for the bare steel wire, up to the 10th mode: error bars (unless plotted) are smaller than symbol size. The linearity of this relation comes from the continuous medium. (b) Residuals of the measured angular frequencies against the fit.

be seen that the relationship between the wavevector and measured frequency agrees with a linear fit. Five repeated measurements were performed for the 1st, 5th, and 10th data point to determine the error, which was on the order of 1 s^{-1}. This is comparable to the symbol size and therefore error bars are obscured in Figure 5. The five arbitrary locations along the mount were chosen to be 220, 190, 150, 130, and 100 cm.

From Figure 5 (b), it is apparent that the 5th and 10th modes deviate most from the linear fit. This can be attributed to the method used to determine the experimental error of the setup, which ultimately affected the results. Namely, the error was calculated by varying the position of the detector along the steel wire and repeating the measurement process for each detector position. In theory, the resonance frequency should not depend on where the detector is placed. However, it is evident that taking the mean of the resonance frequencies as opposed to the value at one position resulted in a significantly different recorded frequency, which is certainly a suboptimal outcome for the first step of the project. The conclusion to draw from this result is that the detector position does indeed have an effect on the ability of the lock-in amplifier to measure resonance frequency, or of the user to locate this frequency. An explanation for this

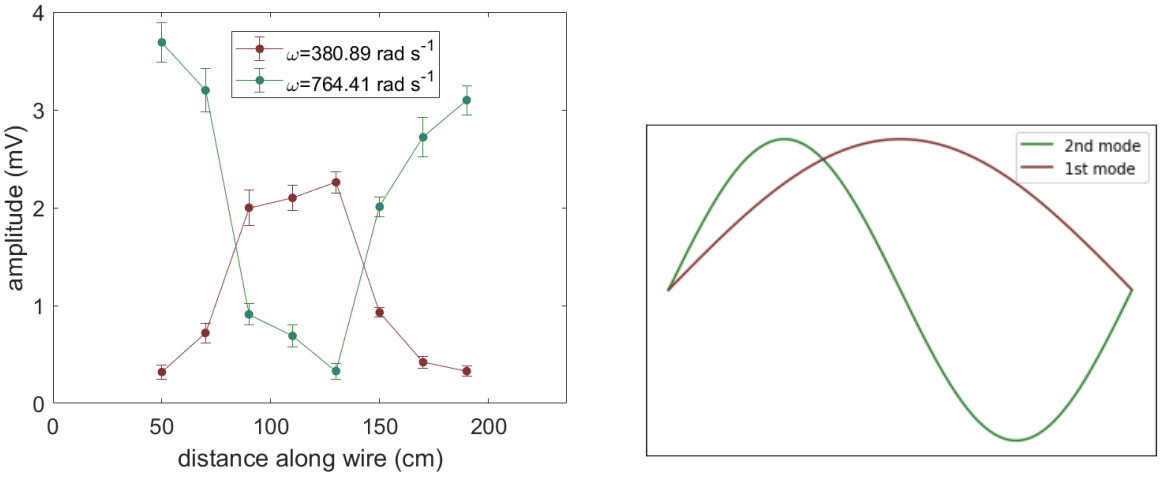

(a) (b)

Figure 6: a) Amplitude of oscillations versus position along the wire, showing the nodal features of the vibrations: the first normal mode is measured to be at $\omega = 380.89$ rad s^{-1}, while the second is at $\omega = 764.41$ rad s^{-1} (See Figure 5.) b) Qualitative diagram of first 2 normal modes of vibration for a string of finite length.

phenomenon was not pursued in this project, but it is substantial enough to note for future attempts at recovering the linear dispersion relation.

The slope from the linear regression was compared to the theoretically predicted value of the phase velocity, $\sqrt{T/\mu}$. This leads to a result for the mass per unit length, $\mu = (6.02 \pm 0.23) \times 10^{-4}$ kg m^{-1}, while the measured diameter of the steel wire is 0.32 ± 0.01 mm. Thus, the mass density of the steel wire is determined to be $\rho = (7485.26 \pm 750.5)$ kg m^{-3}, which is in rough agreement with the reported mass density of steel, between 7750-8100 kg m^{-3}[28]. The linear dispersion is expected to adopt a periodic, non-linear form upon adding beads to the system.

As a final remark, the shapes of the modes were verified by adjusting the position of the detector along the steel wire. These measurements show the nodal features of the first and second modes and are displayed in Figure 6. The singular peak for the first driving frequency indicates that it does indeed correspond to the first mode of vibration, and likewise for the second driving frequency which has 2 peaks.

3 Monatomic Basis

3.1 Phonons

As mentioned earlier, quantized vibrations in solids, known as phonons, play an important role in the origins of various macroscopic behaviour including heat capacity and superconductivity. The normal modes of these vibrations behave as independent quantum harmonic oscillators, and applying a Bose-Einstein statistical treatment to a collection of these excitations is sufficient to predict some of the thermodynamic properties of the material[2].

For example, the Debye model assumes a linear dispersion relation in the phonons, such that all modes characterized by wavevectors have the same speed v_s[2]. Solving for the corresponding density of states in 3-D gives a distribution of frequencies which can be used to calculate the heat capacity of the system and explain the experimentally observed T^3 dependence at low temperatures for many solids[2, 5]. However the dispersion relation for vibrations in lattices is incorrect under the Debye model[2, 1]. The linear approximation holds only in the long wavelength limit, and a suitable treatement of the lattice vibrations must take into account the discreteness of the medium through which they propagate. The resulting periodic dispersion can be demonstrated through a 1-D monatomic chain with linear interactions between neighbouring atoms, all having mass M.

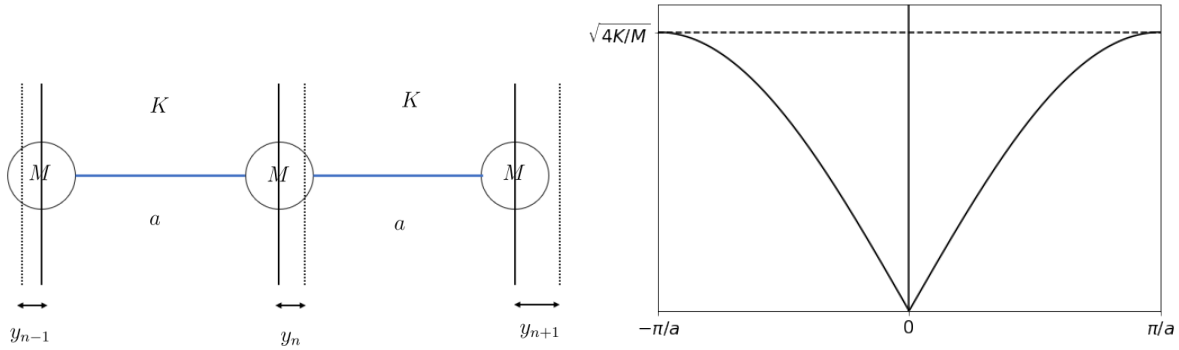

Figure 7: a) 3 elements in a 1-D monatomic chain with lattice parameter a, force constant K, and masses M. b) 1-D monatomic dispersion relation for the monatomic basis.

The following is a standard tratement of lattice vibrations with a monatomic basis. (See Ashcroft and Mermin for one such treatment[12].) Let the displacement from equilbrium of the nth atom be denoted $y_n(t)$. Then, working under the assumptions of the harmonic approximation and Born-von Karman boundary conditions[12] in the monatomic chain, solutions will have the form

$$y_n(t) \propto e^{i(kna-\omega t)},\ k = \frac{2\pi n}{Na},\ n \in \mathbb{Z},\ n \leq N \tag{5}$$

where a is the distance between neighbouring atoms (lattice parameter), N is the number of atoms, and k, ω are the usual parameters of a propagating wave. (See Section 2.1.) The equation of motion for the nth atom is given by the forces acting on it (see Figure 7), where the force constant is given by K

$$M\ddot{y}_n(t) = -K(2y_n - y_{n-1} - y_{n+1}) \tag{6}$$

which, when combined with (5) yields

$$-M\omega^2 e^{i(kna-\omega t)} = -2K(1-\cos(ka))e^{i(kna-\omega t)} \tag{7}$$

Therefore, the excitations occur when

$$\omega = \sqrt{\frac{4K}{M}}|\sin(\frac{1}{2}ka)| \tag{8}$$

which is known as the dispersion relation, $\omega = \omega(k)$ for the 1-D monatomic chain. In the case of the bare string, the dispersion was linear i.e. $\omega = vk$. However, using the discrete elements of the monatomic chain, one finds the wave solutions no longer admit dispersions of this form. Instead, the derivative of the dispersion relation $\frac{d\omega}{dk}$ (the group velocity) goes to zero as $k \to \pi/a$ since $\cos(\pi/2) = 0$. In the 1-D case, this value for the wavenumber marks the edge of the *Brillouin zone*, which is significant in condensed matter physics because such a space is sufficient to characterize all states periodic in the lattice (e.g. phonon frequncies, electron energies)[12].

The resulting "rounding out" of the dispersion relation near the edges of the Brillouin zone is reminiscent of electronic band gaps which occur due to periodic perturbations. The reason for this similarity is not coincidental: non-linearity of the dispersion relation occurs whenever the wavelength of excitations is comparable to the discreteness of the medium. This applies to phonons, electronic wavefunctions and – as this report aims to demonstrate – classical oscillations of weights on a steel wire.

3.2 Experimental setup

For the case of a 1-D monatomic basis, the wire and mount components of the system remain unchanged from the previous setup. The dispersion relation was obtained by attaching beads to the bare wire and placing the driver at one end (22.3 cm from one of the knife edges, as in the bare wire setup). The beads were loaded onto the wire at even intervals specified by the lattice constant a. The lattice constant was chosen to be $a = 0.2363$ m such that 9 beads are required and the length of the wire is divided into 10 regions of equal length. Measurements of the masses of the beads using a digital scale gave an average mass of $\bar{m} = (1.26 \pm 0.06)$ g.

Error calculations are performed in a similar fashion to those from the bare wire setup. The position of the detector is adjusted to be in close proximity to the location of a bead, and the results from different positions yield a value for the uncertainty of the measurement from the lock-in amplifier. As in the bare wire setup, output amplitudes are read from the lock-in amplifier to determine resonance frequencies. Additionally, the measured response of the phase and amplitude versus frequency for one of the beads was determined using the amplitude and phase readings from the lock-in amplifier. In this case, errors on the values of these quantities were taken to be the highest and lowest value observed over a period of time. Due to the analog nature of the device and reading of the values, the error determination was not rigorous.

Mode verification (see Figure 6) was not performed in this experiment and the sequence of detected resonance frequencies is assumed to correspond with the sequence of modes.

3.3 Results

The theoretical dispersion relation is given by

$$\begin{aligned} \omega &= \sqrt{\frac{4T}{ma}} \sin\left|\frac{1}{2}ka\right| \\ &= A \sin\left(\frac{\pi n}{20}\right), \ n = 1, 2, ..., 9 \end{aligned} \tag{9}$$

where a is the 1-D lattice constant (or the separation between beads in this case), and m is the mass of an individual basis element (a bead in this case). Comparing to (8), the effective force constant is seen to be T/a. This comes from the equation of motion for a single bead based on its displacement angle θ from equilibrium, which is (to first-order)

$$\begin{aligned} m\ddot{y} &= T \sin\theta \\ &= \frac{Ty}{a} \end{aligned}$$

so that the force constant is $K = T/a$ as claimed.

Figure 8 displays the measured resonance frequencies of the system against wavenumber. Once again, the error bars are comparable in size to the markers and were omitted. The plot reveals a non-linear dispersion relation in the first Brillouin zone. Indeed, the deviation from linear dispersion was present in the bare string system as well, but since the string contains orders of magnitude more discrete elements (atoms), no noticeable curvature appears. The non-linearity would show near the edge of the Brillouin zone, but this quantity goes to infinity as the lattice constant goes to zero (as in the case of atoms in a wire) and therefore was outside the range of modes plotted ($k_{max} = \pi/a, \ a \to 0 \implies k_{max} \to \infty$).

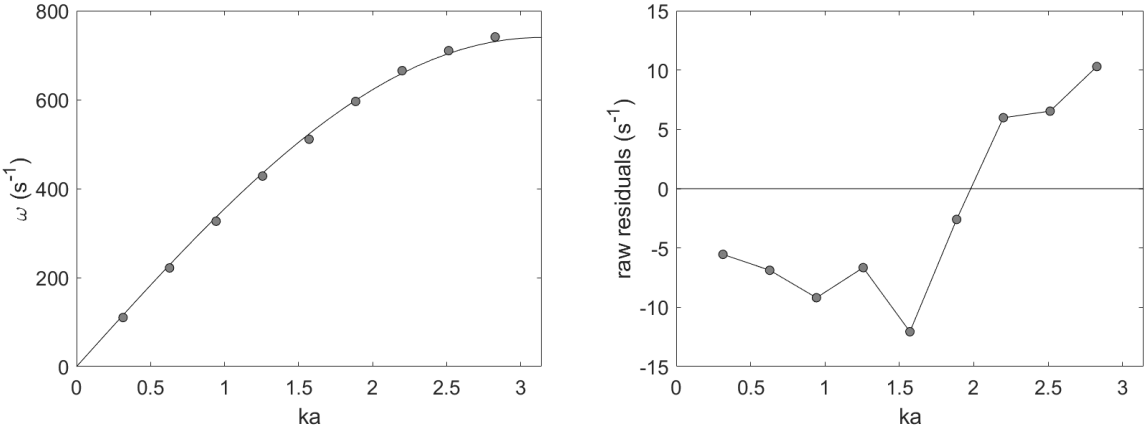

(a) (b)

Figure 8: (a) Measured resonance frequencies of the 1-D lattice system with a monatomic basis. Error bars (unless plotted) are smaller than symbol size. (b) Residuals of the frequencies

The measured response of the phase and amplitude versus frequency for the bead at position 197 cm along the mount (7th bead) is shown in Figure 9. The bead oscillates in a manner that is consistent with a system being driven at its resonance frequency: there is a sharp Lorentzian

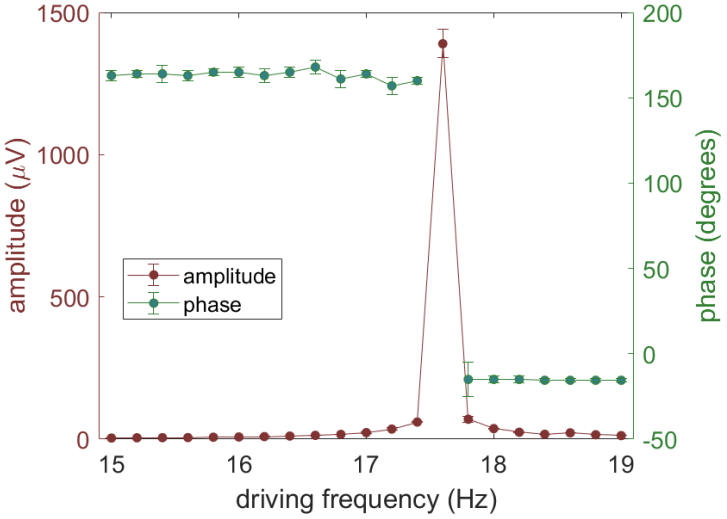

Figure 9: Amplitude and phase versus driving frequency for the 7th bead (position ~ 197 cm) along the monatomic basis setup. The peak at 17.6 Hz corresponds to an eigenfrequency of $\omega = 110.6\ \mathrm{rad\,s^{-1}}$, the frequency of the first normal mode for the monatomic basis system.

peak at the frequency corresponding to the first eigenfrequency (previously determined to be $\omega = 110.6\ \mathrm{rad\,s^{-1}}$ or $f = 17.6$ Hz from the results in Figure 8), and a phase difference of approximately 180 degrees occurs at this point. The phase at a driving frequency of exactly 17.6 Hz is omitted because the phase reading from the lock-in amplifier did not stabilize around a particular value.

Returning to the results obtained for the monatomic dispersion relation, it was determined by fitting a curve to the data that $A = (749.9 \pm 10.0)\ \mathrm{s^{-1}}$. Comparing to the theoretical value of $A = \sqrt{4T/ma} = (811.35 \pm 4.75)\ \mathrm{s^{-1}}$, there is a discrepancy between the predictions and measured data. This discrepancy may be attributed to the finite mass of the steel wire which was assumed to be massless in the theoretical analysis. By treating the mass of a line segment, μa, as a contribution to each bead mass, one achieves better agreement with the experimental results:

$$\begin{aligned} A &= \sqrt{\frac{4T}{(m+\mu a)a}} \\ &= (769.05 \pm 21.90)\ \mathrm{s^{-1}} \end{aligned}$$

where μ comes from the results of Section 2.4. However, merely adding the mass of a segment of the wire to an effective mass term cannot fully reconcile the difference between experiment and theory. This is elaborated using the approximate theoretical results in Section 3.4.

3.4 Numerical Analysis

It is possible to calculate the normal modes and equations of motion for the monatomic system using numerical techniques for solving the eigenvalue problem, and an overview of the procedure for doing so is presented in Appendix A. For example, MATLAB can calculate the eigenvalues and eigenvectors of a matrix using iterative techniques[29] and therefore has the capability of solving for the normal modes of an arbitrary setup of beads. In this section,

the results of implementing a program to calculate normal modes of periodic beads on a taut, massless string are presented and compared to the measurement data for the real system. These results make evident the need to account for the finite mass of the string, and a naive approach to compensate for this difference is shown to improve the agreement between theory (numerical calculations) and experiment. Namely, the finite mass of a segment of string between 2 beads is added to the masses which serve as inputs to the program. (The code for this program is included in Appendix B.)

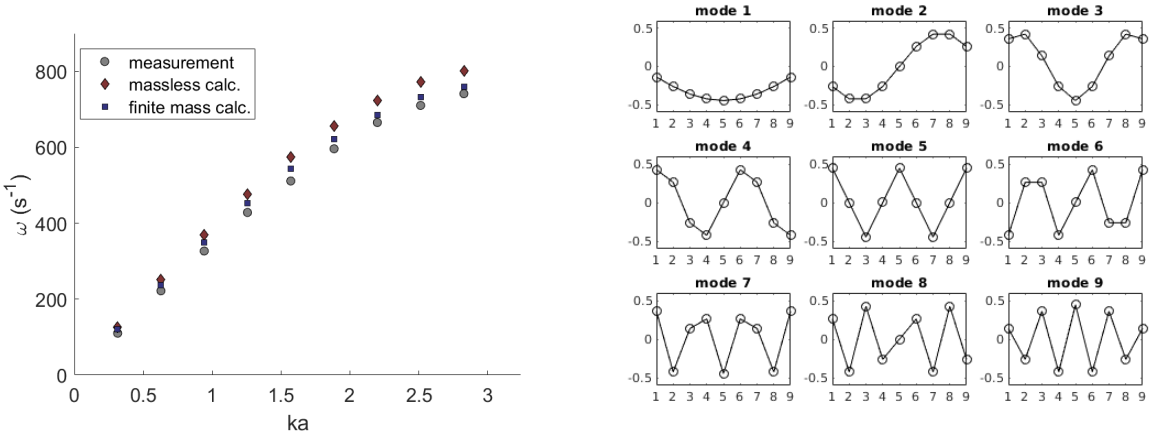

(a) (b)

Figure 10: a) Normal mode frequencies of the system of beads representing the monatomic basis. Results under the assumption of a massless string deviate more strongly than those for which a correction term is added to the bead masses. b) Normal mode shapes for the 9 bead system with a monatomic basis setup.

Figure 10 shows the results of calculating the eigenvalues both by ignoring the mass of the string and by including a correction to the bead masses equal to the weight of the segment between the beads. The linear mass density used as input to calculate this quantity was taken from the results in Section 2.4, $\mu \approx 6.02 \times 10^{-4}$ kg, and the correction term is added as

$$\begin{aligned} m_{eff.} &= \bar{m} + \mu a \\ &\approx 1.26 \times 10^{-3} + (6.02 \times 10^{-4})(0.2363) \\ &\approx 1.40 \times 10^{-2} \end{aligned}$$

The corresponding results for incorporating this finite mass of the string are in better agreement with the experimental results, although there is still a slight discrepancy which can be attributed to the simplification of adding an effective mass term instead of reformulating the problem as being beads on a *massive* string. In such a model, the string is neither massless nor simply a contribution to the mass of the beads. Instead, a description involving transfer matrices and bays of the system is more appropriate as in the work by Ottarsson and Pierre[19], and this is described in Section 5.

4 Diatomic basis

4.1 Optical and acoustic modes

In many real solids, phonons come in 2 varieties corresponding to 2 classes of solution available when the basis consists of more than one atom, which are known as the *acoustic* and *optical* branches[12]. In the 1-D diatomic case, these 2 distinct dispersion relations arise due to the pair of coupled equations for the atomic displacements y, u of masses M, m corresponding to the 2 atoms in a basis element:

$$\begin{aligned}(2K - M\omega^2)y - K(1 + e^{-ika})u = 0\\ -K(1 + e^{ika})y + (2K - m\omega^2)u = 0\end{aligned} \tag{10}$$

which originates from a similar analysis to that in Section 3.1 except with two different masses in a single basis element. The lattice parameter a matches the periodicity of the structure which is now the distance between 2 atoms of the *same* type. (See Figure 11.) The system of equations (10) admits a solution for two possible values of ω:

$$\omega^2 = K\left(\frac{1}{M} + \frac{1}{m}\right)\left[1 \pm \sqrt{1 - \frac{4mM}{(M+m)^2}\sin^2(ka/2)}\right] \tag{11}$$

which are shown in Figure 11. At the edges of the Brillouin zone, there is a bandgap between the optical and acoustic branches. The lower branch has the same structure[12] as the dispersion relation for the monatomic basis and, for small k is approximately linear in k such that $\omega = vk$. For this reason, it is known as the acoustic branch: sound waves propagate with linear dispersion in solids. The top branch is known as the optical branch because the modes with these higher frequencies can interact with light and be probed in this manner[12].

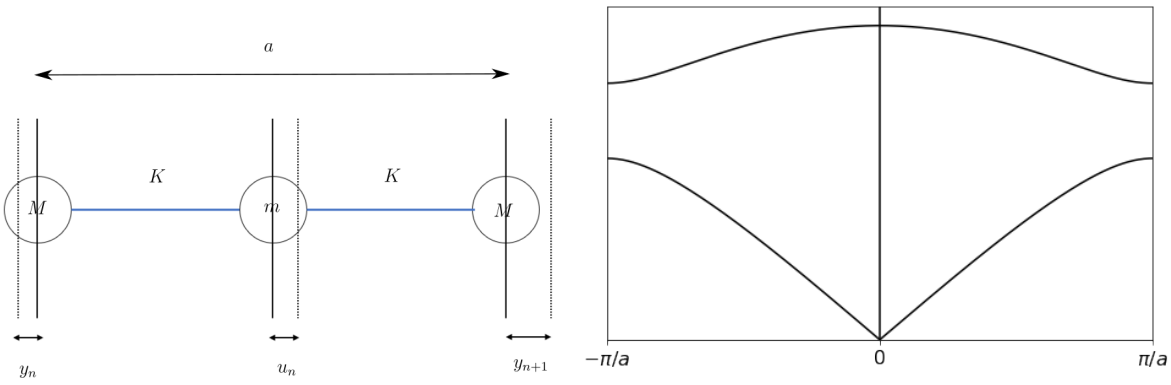

(a) (b)

Figure 11: a) Elements in a 1-D diatomic chain with lattice parameter a and masses M, m. b) 1-D dispersion relation for the diatomic basis.

4.2 Experimental setup

The dispersion relation for a 1-D diatomic lattice was obtained by attaching beads of 2 different sizes in an alternating fashion, equally spaced. In this case, the lattice constant a is the distance of one repeating unit (i.e. 2 times the distance between neighbouring beads). For this setup of the experiment, a is chosen to be 0.4296 m such that 5 basis elements (10 beads)

are placed on the string and the wire is divided into 11 regions of equal length. A second size of bead is selected and measured to be $\bar{m} = 0.73 \pm 0.11$ g. The beads from the monatomic setup of mass 1.26 ± 0.06 kg are now denoted by $\bar{M}$. Error calculations are performed in a similar fashion to the bare string and monatomic basis setups. The position of the detector is varied to obtain multiple resonance frequency measurements and yield a value for the measurement error. Once again, mode verification (see Figure 6) was not performed in this experiment. The sequence of detected resonance frequencies is assumed to correspond with the sequence of modes.

4.3 Results

The theoretical dispersion relation in the case of a diatomic basis is given by

$$\begin{aligned}\omega &= \sqrt{\frac{2T}{a}\left(\frac{1}{m}+\frac{1}{M}\right)\left[1 \pm \sqrt{1-\frac{4mM}{(M+m)^2}\sin^2(ka/2)}\right]} \\ &= \sqrt{A\left[1 \pm \sqrt{1-B\sin^2(\pi n/11)}\right]},\ n = 1, 2..., 5 \end{aligned} \tag{12}$$

where a, m, and M are as described in Section 4.2, and $ka = \frac{2\pi n}{11}$ because the beads divide the wire into 11 equal segments and one basis element consists of 2 segments. Also, the force constant for the interaction between the masses is $K = 2T/a$ since the distance between the neighbouring masses is now $a/2$.

Figure 12 shows the measured frequencies of the system against the wavenumber, similar to the previous section. The error was once again on the order of the symbol size. In this case, one must consider modes corresponding to acoustic and optical branches within the first Brillouin zone, which in 1-D is just the cut-off wavenumber $k_{max} = \pi/a$. The acoustic dispersion resembles the results from the monatomic basis, in that there is a rounding out of the relation as the wavevector approaches the edge of the Brillouin zone.

As in the work by Lüerßen *et al.*[8], there is a slight discrepancy between the optimal parameters A, B obtained from the data and the theoretical values that would be obtained from known experimental parameters like the lattice constant, bead masses, and tension. This is because the finite mass of the wire has an appreciable effect on the behaviour of the system, especially for the optical modes, which is elaborated in Section 4.4. By simultaneously fitting the expressions for the optical and acoustic dispersion relations, a value of $A = 4.41 \times 10^5$ s^{-2} is obtained using numerical root solving. (In this case there is no confidence interval associated with the curve-fitting answer so there is no error provided.)

The fit underestimates the theoretical value for the parameter, $A = \frac{2T}{a}(\frac{1}{M} + \frac{1}{m})$, which is $A = (4.94 \pm 0.61) \times 10^5$ s^{-2} under the assumption of a massless wire and using the system parameters. However, one could once again achieve better agreement between the theoretical value and the fit by incorporating a contribution to the effective mass from the wire segements within a basis element. For a proof of concept result (using approximate values for parameters), one can add a value of $\mu a/2 \approx 1.29 \times 10^{-4}$ kg to both masses m and M, and calculate the new theoretical value to be

$$\begin{aligned} A &= \frac{2T}{a}\left(\frac{1}{M+\mu a/2}+\frac{1}{m+\mu a/2}\right) \\ A &\approx 4.30 \times 10^5 \text{ s}^{-2} \end{aligned} \tag{13}$$

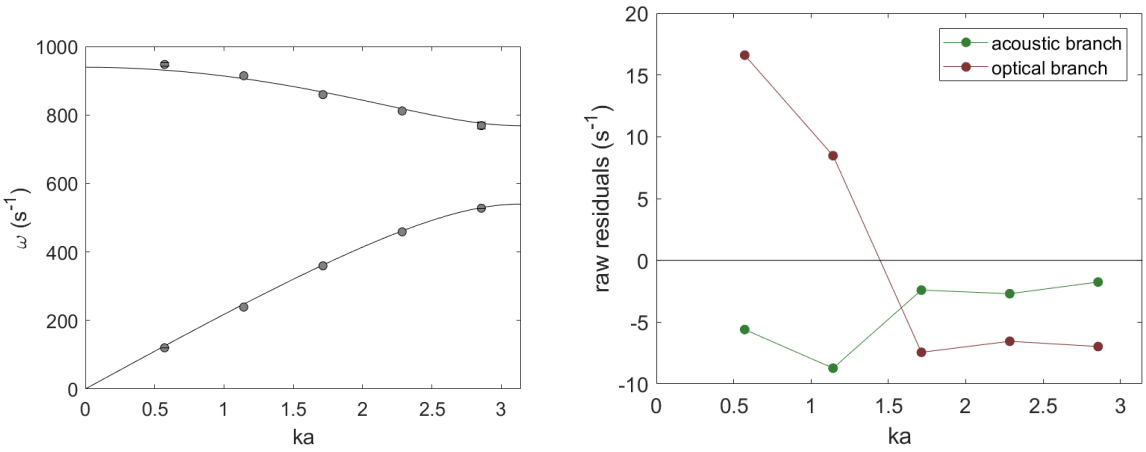

(a) (b)

Figure 12: (a) Dispersion relation for the diatomic basis, up to the fifth wavenumber in the discrete system. Error bars (unless plotted) are smaller than symbol size. There is an optical and acoustic branch at higher and lower frequencies respectively, corresponding to different vibrational modes, and these correspond nicely to a fit using the above dispersion relation. (b) Residuals of the measured angular frequencies against the fit.

Although this is closer to the value obtained from experimental data, there is still a slight discrepancy.

4.4 Numerical Analysis

Similar to the monatomic basis system, one can solve numerically for the eigenvalues of the periodic system under the assumption of a massless string and compare the results to the data. (See Appendix B for the code.) Then, the effective mass of the beads can be adjusted to include an additional contribution from the segment of the wire between neighbouring beads, $\mu a/2$. Each bead – heavy or light – receives this additional contribution to its mass. The results of the calculations are shown in Figure 13.

The experimental results for the optical branch frequencies are recovered quite nicely. However, the discrepancy is visible for higher modes of the acoustic branch, for which the calculations overestimate the results obtained from the lock-in amplifier. Once again, although the approximation of a massless string is inaccurate, the deviation from experimental results is not fully explained by adding a contribution to the effective mass of the beads. The optical modes appear to deviate most. A different model for the dynamics of the system is required. (See Section 5.)

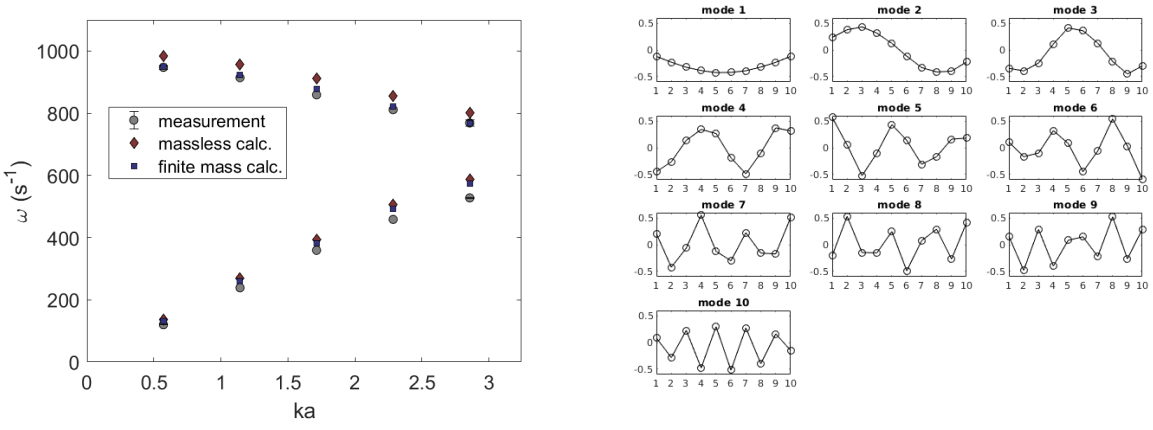

(a) (b)

Figure 13: a) Normal mode frequencies of the system of beads representing the diatomic basis. As in the monatomic case, results under the assumption of a massless string deviate most from the experimental results. b) Normal mode shapes for the 10 bead system with a diatomic basis setup.

5 Anderson Localization

5.1 Localization effects in solids

This section provides a brief overview of the mechanism behind Anderson localization and its relationship to mechanical excitations as in the case of a beaded steel wire. In 1958, P.W. Anderson posited that randomness in the lattice could be responsible for a complete disappearance of electron diffusion[13], and later this was extended to provide an explanation for the metal-insulator phase transition[30]. The phenomenon is attributed to the wave-like nature of electrons, which become localized when travelling through a disordered medium. If a lattice exhibits spatial periodicity, the electrons are able to tunnel from site to site unimpeded in a Bloch state[14]. However, upon reaching a critical level of disorder the scattered waves interfere destructively away from the original lattice site such that the wave amplitude decays exponentially and the electron is overwhelmingly likely to be confined to a single region[16]. For an example closer to the work in this report, destructive interference was recently shown to cause localization of heat conducting phonons in experiment (using nanodots)[25].

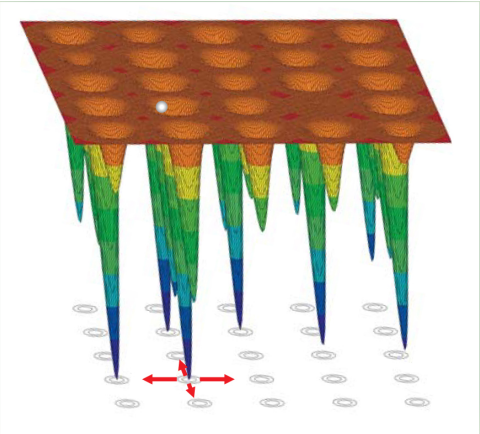

Figure 14: Electron hopping on a 2-D lattice with random potentials. Red arrows show possible hopping directions (via tunnelling). A critical amount of disorder localizes the electron[22].

Anderson originally proposed a tight-binding model[12] whose Hamiltonian takes the following form in second quantization for spinless electrons[17, 31]

$$\hat{H} = W \sum_i \epsilon_i \hat{c}_i^\dagger \hat{c}_i + t \sum_{<i,j>} (\hat{c}_i^\dagger \hat{c}_j + h.c.) \tag{14}$$

where $< i, j >$ is the index for the nearest neighbours of site i, $\epsilon_i \in [-1/2, 1/2]$ is the on-site energy, t parametrizes the hopping, and W is the disorder parameter. In 1-D, the eigenstate of the Hamiltonian is given by summing over every site, $|\Psi\rangle = \sum_i \psi(i)|i\rangle$, where $\psi(i)$ is the wavefunction at site i and $|i\rangle$ is a state representing the presence of a particle at the site[31]. Setting $t = 1$ and $W = 1$ and using the time-independent Schrodinger equation $\hat{H}|\Psi\rangle = E|\Psi\rangle$ one obtains a recursive relationship for the wavefunctions at site i[17]

$$E\psi(i) = \epsilon_i \psi(i) + \psi(i+1) + \psi(i-1) \tag{15}$$

which can then be rewritten

$$\begin{pmatrix} \psi(i+1) \\ \psi(i) \end{pmatrix} = \mathbf{T}_i \begin{pmatrix} \psi(i) \\ \psi(i-1) \end{pmatrix}, \quad \mathbf{T}_i = \begin{pmatrix} E - \epsilon_i & -1 \\ 1 & 0 \end{pmatrix} \tag{16}$$

Here, $\mathbf{T}_i$ is the transfer matrix for the propagation of amplitudes from site to site, which is formed by the *random* parameter ϵ_i. Finally, by chaining these transfer matrices together, one finds the amplitude at the nth site to be

$$\begin{pmatrix} \psi(n) \\ \psi(n-1) \end{pmatrix} = \prod_{i=1}^{n-1} \mathbf{T}_i \begin{pmatrix} \psi(1) \\ \psi(0) \end{pmatrix} \tag{17}$$

which yields a *particular* solution of the wavefunction[17]. Now, by Fuerstenbergs theorem for random matrices[32, 17], the overall effect of the random hopping is a localization of the state $|\Psi\rangle$ whereby, for sufficiently large n

$$\psi(n) \sim e^{-n/\xi} \tag{18}$$

ξ is known as the localization length, and if the system size reaches the threshold value $n > \xi$, there is an absence of diffusion. The electrons in this case are said to be localized.

It is known from work such as Mott and Twose[33] that almost all eigenstates tend to be localized in 1-D systems. Though not obvious, the existence of localized eigenstates follows from the exponential growth of the wavefunction as in (18) according to Ishii[17]. (This is not proven rigorously in this report, but is given quite nicely by Ishii.) In fact, the statement for 1-D systems is much stronger than an existence claim: for large enough systems, every eigenstate becomes localized[17, 31]. This is because, regardless of the value of the disorder parameter $W \neq 0$, 1-D systems exhibit localization for n greater than some ξ depending on the parameters of the system. Figure 15 shows the relationship between disorder and localization through the results of a Monte Carlo simulation with $E = 0$, $t = 1$ (the code for which can be found in Appendix C). In contrast, the eigenstates of higher-dimensional systems are not localized until a critical level of disorder is reached[14, 13, 31], characterized by W_c. It is this critical disorder which is theorized to mark the metal-insulator phase transition in real solids[30].

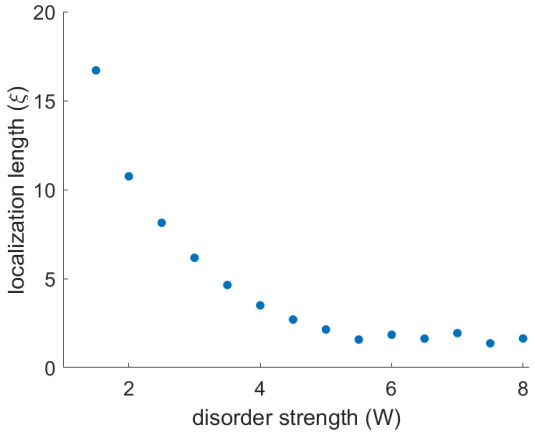

Figure 15: Results of a Monte Carlo simulation for which W is varied and ξ determined by applying random transfer matrices as in (16) $n = 1000$ times, fitting an exponential function, and then taking the average from 100 results at each W. $E = 0$ and $t = 1$ throughout, and the initial state is chosen to be $\psi(0) = 1$, $\psi(1) = 1$ similar to the work in[31].

More generally, localization effects are present in nearly any structure upon introducing disorder[17]. For example, localized modes of vibrations occur in materials with structural defects.

This can sometimes lead to unfortunate consequences due to the energy of excitations being confined within the general area of the source[23, 24]. (It is a historical curiosity that the study of localization in quantum systems predates interest in localized acoustic waves.) The system of beads on a wire studied in this report serves as a suitable demonstration of localized modes. Before constructing such modes, however, it is instructive to rephrase the dynamics of the beads on wire in terms of transfer matrices as well.

By taking into account the dynamics of the string in addition to the beads, one can conceive of a transfer matrix formulation of the bead displacements (See Ottarsson and Pierre[19])

$$\begin{pmatrix} y_i \\ y_{i-1} \end{pmatrix} = \mathbf{Z}_{i,i-1} \begin{pmatrix} y_{i-1} \\ y_{i-2} \end{pmatrix}, \ \mathbf{Z}_{i,i-1} = \begin{pmatrix} \beta_{i,i-1} & -\alpha_{i,i-1} \\ 1 & 0 \end{pmatrix} \tag{19}$$

where $\beta_{i,i-1}, \alpha_{i,i-1}$ are parameters depending on the bead masses and separations. By randomizing these parameters, and noting the resemblance with (16), one reaches the result once again that

$$y_n \sim e^{-n/\xi} \tag{20}$$

A rigorous proof of this formulation is less important than noticing the qualitative similarities between wave propagation in this situation and in the case of 1-D electrons. In accordance with the statement that disorder leads to localization, a similar result applies in both cases, and localized eigenstates are expected to occur in the beaded wire system. These are explored in the following sections.

5.2 Predicting eigenstates in disordered media

While diagonalizaing an arbitrary matrix is susceptible to numerical error, this is negligible for small systems. For example, looking at a system of 7 beads (as in Ottarsson and Pierre[19]) the localized eigenstates of the system can be computed directly and the corresponding mode shapes determined in this fashion. By varying the separations randomly and solving for the normal mode shapes, localized eigenstates are discovered.

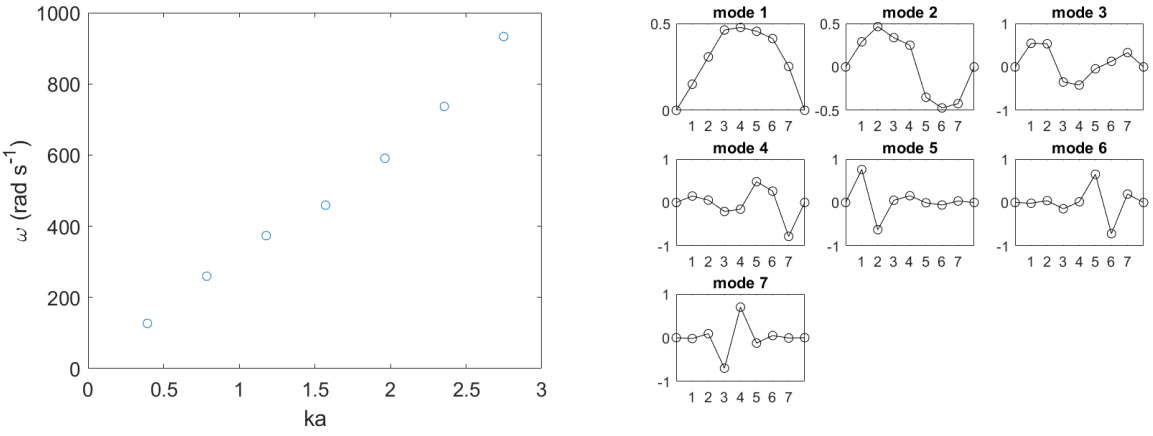

(a) (b)

Figure 16: Localized mode shapes in a system of 7 beads with separations drawn from the distribution $l_i = 29.54(1 + \delta_i)$ cm, $\mathrm{Var}[\delta_i] = 0.05$, $\mathrm{E}[\delta_i] = 0$.

Figure 16 shows a particular set of mode shapes and frequencies when the setup consists of beads of mass $m = 1.26$ g, tension as in the setup from the previous sections, and separations given by $l_i = 29.54(1 + \delta_i)$ cm. The random variable δ_i has zero mean and variance 0.05. In this instance, modes 5-7 are localized. The mode shapes varied across multiple setups as the separations changed; however, they were qualitatively similar in that most configurations resulted in some localized modes. Figure 17 shows how localization becomes more pronounced upon adding more beads. The mode shapes for modes 400-408 (in order of increasing eigenfrequency) are shown for a system of 500 beads with $l_i = 29.54(1 + \delta_i)$ cm. δ_i has mean zero and variance 0.08, and the mass and tension are kept the same.

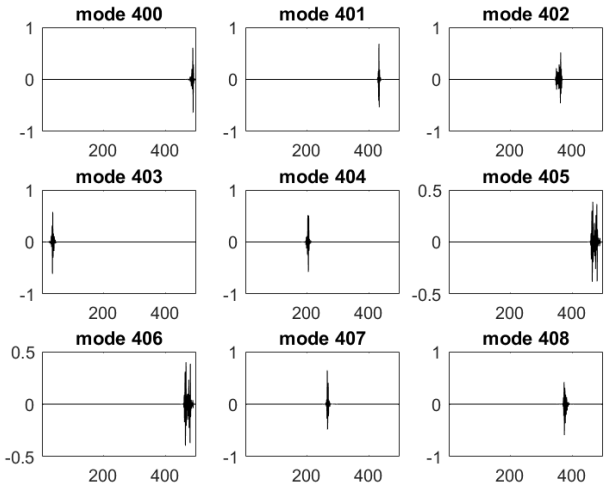

Figure 17: Localized mode shapes in a system of 500 beads with separations drawn from the distribution $l_i = 29.54(1 + \delta_i)$ cm, $\mathrm{Var}[\delta_i] = 0.08$, $\mathrm{E}[\delta_i] = 0$.

5.3 Experimental setup

While the 500 bead setup would yield striking results, it is highly impractical to implement. The 7 bead system, however, is feasible and the approximate setup used to produce Figure 16 was adopted in the steel wire and bead system. Prior to configuring the physical system, the calculations were repeated after normalizing the lengths to sum to 2.363 m and adding an effective mass contribution of $\mu L/8$ to each bead. (This can be seen as an average contribution in this case, since the separations are different.) These adjustments yielded eigenfrequencies of 590.98 rad s^{-1} for the 5th normal mode shape, and 933.21 rad s^{-1} for the 7th normal mode shape in Figure 16. The intention was then to verify the presence of these mode shapes at approximately these eigenfrequencies in the physical system using the lock-in amplifier.

The driving frequency was tuned around 47.03 Hz and then 74.26 Hz in accordance with the 2 eigenfrequencies above, accounting for the necessary 2nd harmonic reference frequency. The resonances should have been located around these values and once found, they were kept fixed. The positions of the beads were fixed at separations of 24.77, 29.38, 39.73, 8.82, 40.45, 15.57, 34.46, and 43.12 cm in sequence, and the detector was placed near each of their positions. Similar to the procedure outlined in Section 2.3, the error for the amplitude readings against position was obtained by choosing the most frequently displayed value for the output voltage and recording the largest deviation from this value.

5.4 Results

Resonances for the two modes were found at 43.70 Hz and 73.51 Hz in rough agreement with the calculated values above. These were expected to correspond to the 5th and 7th mode shapes, respectively, taken from Figure 16. The agreement with the qualitative shapes of these modes is quite good, as can be seen in Figure 18. The driver is kept a distance of 22.3 cm along the wire throughout. In Figure 18 a), the 1st and 2nd beads oscillate with the highest amplitudes, and this vibration attenuates along the wire. Although phase data, if recorded, would have made the mode shape clearer, the plot is in agreement with the 5th mode of Figure 16 in which the 1st and 2nd beads oscillate out of phase and the rest are mostly stationary. In Figure 18 b), the 3rd and 4th beads have the highest amplitudes, agreeing with the 7th mode shape in Figure 16. In summation, the localized mode shapes are verified at approximately the frequencies calculated to be the corresponding eigenfrequencies.

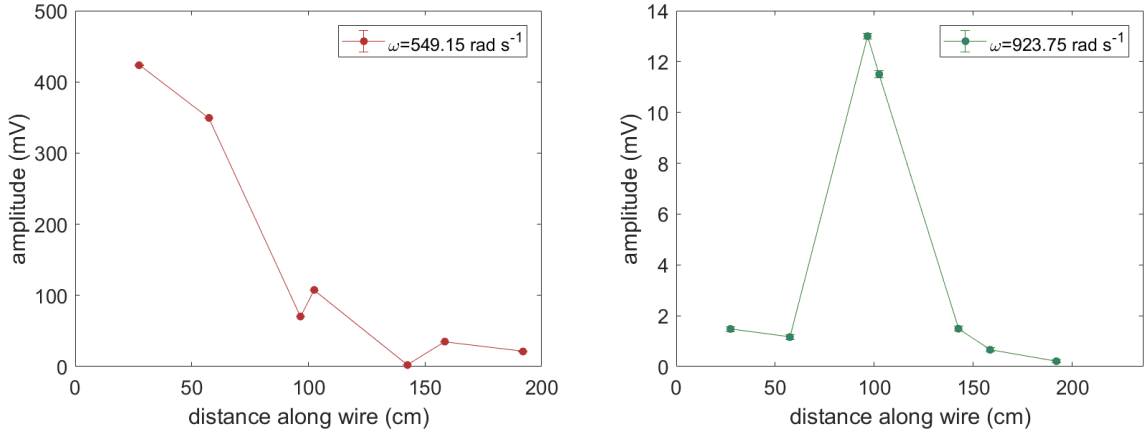

(a) (b)

Figure 18: a) Measured amplitudes against position showing the localized mode shape for the 5th mode. Error bars smaller than symbol size unless shown. b) Localized mode shape for the 7th mode.

5.5 Beyond the first passband

As a final demonstration, localization beyond the first passband was investigated according to the framework developed by Ottarsson and Pierre[19]. Treating the wire as a 1-D massive medium instead of a massless distance between the beads allows for the expression of more complex eigenstates beyond the first n modes in an n bead system. These higher modes are called passbands, corresponding to a family of solutions to the transfer matrix problem which do not attenuate. For example, one possible eigenstate in the case of periodic beads involves mode shapes in which the beads are motionless, but the segments of wire *between* the beads oscillate out of phase. This is the first mode of the second passband, and it is not accounted for in the previous model.

Localized modes of vibration between the beads was explored: the analogy between the localization of a continuous mechanical wave and electron wavefunction is stronger than in the case of discrete bead elements. For a fixed driving frequency of 166.38 Hz, localization between the 7th bead and knife-edge was found (similar to the mode shapes in Figure 2 (a) in the introduction of this report). To verify the localization, the detector was placed in the middle

of each wire segment between 2 beads and the amplitude at these positions was recorded. The results of these measurements are shown in Figure 19.

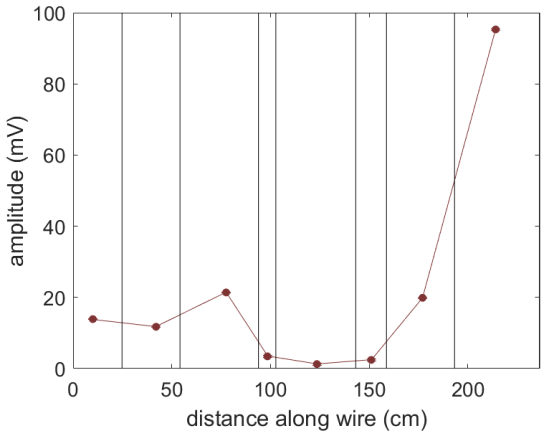

Figure 19: Localized mode in higher passband, with driving frequency 166.38 Hz. The vertical lines denote the positions of the beads along the mount. It is apparent that the continuous mechanical wave travelling along the wire is localized between the 7th bead and the end of the wire (the knife-edge).

For future consideration, these higher passbands could be explored further and the behaviour of the continuous 1-D wave in relation to the localization of the electronic wavefunction addressed more carefully.

References

[1] Charles Kittel and Paul McEuen. *Introduction to solid state physics*. Wiley, 2018.

[2] Stephen Blundell and Katherine Blundell. *Concepts in thermal physics*. Oxford University Press, 2009.

[3] Franz Schwabl. *Advanced quantum mechanics. -4th ed.* Springer, 2008.

[4] Joseph Callaway. "Model for Lattice Thermal Conductivity at Low Temperatures". In: *Physical Review* 113.4 (1959), pp. 1046–1051. DOI: 10.1103/physrev.113.1046. URL: https://doi.org/10.1103/physrev.113.1046.

[5] R. Stedman, L. Almqvist, and G. Nilsson. "Phonon-Frequency Distributions and Heat Capacities of Aluminum and Lead". In: *Physical Review* 162.3 (1967), pp. 549–557. DOI: 10.1103/physrev.162.549. URL: https://doi.org/10.1103/physrev.162.549.

[6] J. Bardeen, L. N. Cooper, and J. R. Schrieffer. "Theory of Superconductivity". In: *Physical Review* 108.5 (1957), pp. 1175–1204. DOI: 10.1103/physrev.108.1175. URL: https://doi.org/10.1103/physrev.108.1175.

[7] Walter C. Michels and Norma L. Curtis. "A Pentode Lock-In Amplifier of High Frequency Selectivity". In: *Review of Scientific Instruments* 12.9 (1941), pp. 444–447. DOI: 10.1063/1.1769919. URL: https://doi.org/10.1063/1.1769919.

[8] Dietrich Lüerßen et al. "A demonstration of phonons that implements the linear theory". In: *American Journal of Physics* 72.2 (2004), pp. 197–202. DOI: 10.1119/1.1625923. URL: https://doi.org/10.1119/1.1625923.

[9] Wikimedia Commons. *Phonon propagating through a square lattice*. 2007. URL: https://commons.wikimedia.org/wiki/File:Lattice_wave.svg.

[10] Paolo Giannozzi et al. "QUANTUM ESPRESSO: a modular and open-source software project for quantum simulations of materials". In: *Journal of Physics: Condensed Matter* 21.39 (2009), p. 395502. DOI: 10.1088/0953-8984/21/39/395502. URL: https://doi.org/10.1088/0953-8984/21/39/395502.

[11] *ARCHER UK National Supercomputing Service*. URL: http://www.archer.ac.uk/.

[12] Neil Ashcroft, David Mermin, and Dan Wei. *Solid State Physics. Revised Edition*. Cengage Learning Asia, 2016.

[13] P. W. Anderson. "Absence of Diffusion in Certain Random Lattices". In: *Physical Review* 109.5 (1958), pp. 1492–1505. DOI: 10.1103/physrev.109.1492. URL: https://doi.org/10.1103/physrev.109.1492.

[14] D.J. Thouless. "Electrons in disordered systems and the theory of localization". In: *Physics Reports* 13.3 (1974), pp. 93–142. DOI: 10.1016/0370-1573(74)90029-5. URL: https://doi.org/10.1016/0370-1573(74)90029-5.

[15] Vladimir Dobrosavljevic, Nandini Trivedi, and Jr. James M. Valles, eds. *Conductor-Insulator Quantum Phase Transitions*. Oxford University Press, 2012. DOI: 10.1093/acprof:oso/9780199592593.001.0001. URL: https://doi.org/10.1093/acprof:oso/9780199592593.001.0001.

[16] "The nature of the electronic states in disordered one-dimensional systems". In: *Proceedings of the Royal Society of London. Series A. Mathematical and Physical Sciences* 274.1359 (1963), pp. 529–545. DOI: 10.1098/rspa.1963.0148. URL: https://doi.org/10.1098/rspa.1963.0148.

[17] Kazushige Ishii. "Localization of Eigenstates and Transport Phenomena in the One-Dimensional Disordered System". In: *Progress of Theoretical Physics Supplement* 53 (1973), pp. 77–138. DOI: 10.1143/ptps.53.77. URL: https://doi.org/10.1143/ptps.53.77.

[18] Longyan Gong et al. "A measure of localization properties of one-dimensional single electron lattice systems". In: *Physics Letters A* 380.1-2 (2016), pp. 59–64. DOI: 10.1016/j.physleta.2015.09.036. URL: https://doi.org/10.1016/j.physleta.2015.09.036.

[19] Gisli Óttarsson and Christophe Pierre. "Vibration and wave localization in a nearly periodic beaded string". In: *The Journal of the Acoustical Society of America* 101.6 (1997), pp. 3430–3442. DOI: 10.1121/1.419510. URL: https://doi.org/10.1121/1.419510.

[20] G. Maidanik and J. Dickey. "Localization and delocalization in the response of a beaded string". In: *The Journal of the Acoustical Society of America* 94.3 (1993), pp. 1814–1814. DOI: 10.1121/1.407866. URL: https://doi.org/10.1121/1.407866.

[21] Shanjin He and J. D. Maynard. "Detailed measurements of inelastic scattering in Anderson localization". In: *Physical Review Letters* 57.25 (1986), pp. 3171–3174. DOI: 10.1103/physrevlett.57.3171. URL: https://doi.org/10.1103/physrevlett.57.3171.

[22] Ad Lagendijk, Bart van Tiggelen, and Diederik S. Wiersma. "Fifty years of Anderson localization". In: *Physics Today* 62.8 (2009), pp. 24–29. DOI: 10.1063/1.3206091. URL: https://doi.org/10.1063/1.3206091.

[23] N. A. Valero and O. O. Bendiksen. "Vibration Characteristics of Mistuned Shrouded Blade Assemblies". In: *Journal of Engineering for Gas Turbines and Power* 108.2 (1986), p. 293. DOI: 10.1115/1.3239902. URL: https://doi.org/10.1115/1.3239902.

[24] S.-T. Wei and C. Pierre. "Localization Phenomena in Mistuned Assemblies with Cyclic Symmetry Part I: Free Vibrations". In: *Journal of Vibration Acoustics Stress and Reliability in Design* 110.4 (1988), p. 429. DOI: 10.1115/1.3269547. URL: https://doi.org/10.1115/1.3269547.

[25] M. N. Luckyanova et al. "Phonon localization in heat conduction". In: *Science Advances* 4.12 (2018), eaat9460. DOI: 10.1126/sciadv.aat9460. URL: https://doi.org/10.1126/sciadv.aat9460.

[26] Mary L. Boas. *Mathematical Methods in the Physical Sciences / 2nd ed.: Ill.: Bib.* Wiley, 1983.

[27] *MODEL SR830 DSP Lock-In Amplifier Manual*. 1993.

[28] Glenn Elert. *Density of Steel*. URL: https://hypertextbook.com/facts/2004/KarenSutherland.shtml.

[29] *MATLAB eig documentation*. https://uk.mathworks.com/help/matlab/ref/eig.html.

[30] E. Abrahams et al. "Scaling Theory of Localization: Absence of Quantum Diffusion in Two Dimensions". In: *Physical Review Letters* 42.10 (1979), pp. 673–676. DOI: 10.1103/physrevlett.42.673. URL: https://doi.org/10.1103/physrevlett.42.673.

[31] Daniel Bruns, Rafael Haenel, and Gary Tom. *Anderson localization notes*. https://www.phas.ubc.ca/~berciu/TEACHING/PHYS502/PROJECTS/17AL.pdf. 2017.

[32] H. Furstenberg and H. Kesten. "Products of Random Matrices". In: *The Annals of Mathematical Statistics* 31.2 (1960), pp. 457–469. DOI: 10.1214/aoms/1177705909. URL: https://doi.org/10.1214/aoms/1177705909.

[33] N.F. Mott and W.D. Twose. "The theory of impurity conduction". In: *Advances in Physics* 10.38 (1961), pp. 107–163. DOI: 10.1080/00018736100101271. URL: https://doi.org/10.1080/00018736100101271.

A Beads on a string redux

A brief review of the dynamics of a system of beads on a string is presented to aid in the description of a computational solution to this problem, as in Sections 3.4 and 4.4. We may solve exactly for the equations of motion of a system of n beads on a taut, massless string of length L by obtaining the normal modes of the system and imposing initial conditions such that we end with the expression

$$\mathbf{y}(t) = \sum_{i=1}^{n} \gamma_i \cos(\omega_i t)\mathbf{v}_i \tag{21}$$

where $\mathbf{y}(t)$ is a vector representing the displacements of the beads, the parameters $\{\gamma_i\}$ are determined from their initial displacements, and $\{(\omega_i, \boldsymbol{v}_i)\}$ is the set of eigenfrequencies and corresponding eigenvectors of the system. For example, consider the system with $n = 4$ beads

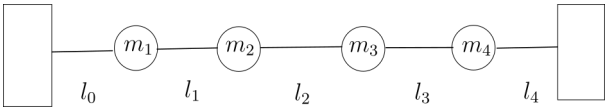

Figure 20: System of 4 beads on a taut, massless string.

suspended on a string with constant tension T and separations $\{l_i\}$ as in Figure 20. When the transverse displacements of the beads are small compared to the separations, we obtain an expression (correct to first-order) for the elongation of the string between segments

$$\Delta l_i = \frac{(y_{i+1} - y_i)^2}{2l_i}$$

so that our potential energy is

$$V(\{y_i\}) = \frac{T}{2} \sum_{i=0}^{4} \frac{(y_{i+1} - y_i)^2}{l_i}$$

where we define the positions at the endpoints to be $y_0 = y_5 = 0$. Treating $\{y_i\}$ as the coordinates of the system and taking the force to be the negative gradient of the potential gives a system of equations where each coordinate is coupled to its nearest neighbours (which makes sense intuitively)

$$\begin{aligned}
m_1\ddot{y}_1(t) &= \left(-\frac{T}{l_0} - \frac{T}{l_1}\right) y_1 + \left(\frac{T}{l_1}\right) y_2 \\
m_i\ddot{y}_i(t) &= \left(\frac{T}{l_{i-1}}\right) y_{i-1} + \left(-\frac{T}{l_{i-1}} - \frac{T}{l_i}\right) y_i + \left(\frac{T}{l_i}\right) y_{i+1}, \ i = 2, 3 \\
m_4\ddot{y}_4(t) &= \left(\frac{T}{l_3}\right) y_3 + \left(-\frac{T}{l_3} - \frac{T}{l_4}\right) y_4
\end{aligned}$$

This can be written succinctly in matrix form

$$\begin{aligned}
&\mathbf{M}\ddot{\mathbf{y}} = \mathbf{K}\mathbf{y} \\
\Leftrightarrow \quad &\ddot{\mathbf{y}} = \mathbf{M}^{-1}\mathbf{K}\mathbf{y}
\end{aligned}$$

where $\mathbf{y}$ is the column vector of bead displacments, $\mathbf{M}$ is a 4 by 4 diagonal matrix of the bead masses, and $\mathbf{K}$ comprises the proportionality constants for the forces acting on each bead

from its own displacement as well as that of its neighbours. Diagonalizing the matrix on the right-hand side gives

$$\ddot{\mathbf{y}} = \mathbf{V}^{-1}\mathbf{D}\mathbf{V}\mathbf{y}$$

where $\mathbf{V}$ is the transformation to the eigenbasis $\{\mathbf{v}_i\}$ and $\mathbf{D}$ is a diagonal matrix of corresponding eigenvalues. The displacements are represented in the eigenbasis as $\mathbf{g} = \mathbf{V}\mathbf{y}$. As such, we may substitute this relation to get 4 independent scalar equations

$$\begin{aligned} &\ddot{\mathbf{g}} = \mathbf{D}\mathbf{g} \\ \Leftrightarrow\ &\ddot{g}_i(t) = \lambda_i g_i(t),\ i = 1, ..., 4 \end{aligned}$$

Identifying λ_i with the angular frequencies $-\omega_i^2$ and setting the initial conditions with zero velocity gives

$$g_i(t) = g_i(0)\cos(\omega_i t)$$

Finally, transforming back to the basis of bead displacements as coordinates and making the assignment $\gamma_i = g_i(0)$ recovers Equation 21. In summary, the computational procedure for determining the equations of motion is

1. Determine matrix $\mathbf{M}^{-1}\mathbf{K}$ based on parameters of system
2. Solve for the eigenvalues to derive the eigenfrequencies and eigenvectors
3. Use initial conditions to determine γ_i

The interesting cases are those solutions which are the result of randomized parameters, as in Anderson localization.

B MATLAB scripts for eigenfrequencies calculation

```
function [ A ] = generate_matrix( tension, n_beads, lengths, weights )
% returns a matrix A describing the motions of the beads
% under the assumption of a massless string and nearest neighbour
% coupling.
% the eigenvectors of A describe the mode shapes,
% while the eigenfrequencies are calculated from the eigenvalues

K = zeros(n_beads,n_beads);
K(1,1) = -tension/lengths(1)-tension/lengths(2);
K(1,2) = tension/lengths(2);
for i=2:n_beads-1
    K(i,i-1) = tension/lengths(i);
    K(i,i) = -tension/lengths(i)-tension/lengths(i+1);
    K(i,i+1) = tension/lengths(i+1);
end
K(n_beads,n_beads-1) = tension/lengths(n_beads);
K(n_beads,n_beads) = -tension/lengths(n_beads)-tension/lengths(n_beads+1);
M = diag(weights);
A = inv(M)*K;
end
```

```
function [ ws, eig_vecs ] = modes( A )
% returns the eigenvectors eig_vecs and
% eigenfrequencies ws of the matrix A describing
% the equations of motion of a beaded string.

 [eig_vecs,eig_vals] = eig(A);
 [ws, ind] = sort(sqrt(-1*diag(eig_vals)));
 eig_vecs = eig_vecs(:,ind);
end
```

C MATLAB script for Monte Carlo simulations of localization lengths

```
n=1000;
Ws = [1:0.5:8];
lls = zeros(1,size(Ws,2));
for k=1:size(Ws,2)
    W = Ws(k);
    if W>4;
        n=500;
    end
    xis=zeros(1,100);
    for j=1:100
        psi = [1; 1];
        psis = zeros(1,n);
        for i=1:n
            T_i = [E - W*(rand(1,1)-0.5), -1;
                   1,                     0];
            psi = T_i*psi;
            psis(i)=psi(2);
        end
        f=fit((1:n).',psis.','exp1');
        xis(j) = 1/f.b; %f.b is inverse of localization length
    end
    lls(k) = mean(xis);
end
```